Modal analysis of elastic vibrations of incompressible materials using a pressure-stabilized finite element method

Ramon Codina[a,*], Önder Türk[b]

[a] *Universitat Politècnica de Catalunya, Barcelona, Spain*
[b] *Middle East Technical University, Ankara, Turkey*

Abstract

This paper describes a modal analysis technique to approximate the vibrations of incompressible elastic solids using a stabilized finite element method to approximate the associated eigenvalue problem. It is explained why residual based formulations are not appropriate in this case, and a formulation involving only the pressure gradient is employed. The effect of the stabilization term compared to a Galerkin approach is detailed, both in the derivation of the approximate formulation and in the error estimate provided.

Keywords: Modal analysis, Incompressible elastic waves, Eigenvalue problems, Stabilized finite element methods

1. Introduction

Analyzing deformations in incompressible solid mechanics has become increasingly important in recent years due to its wide applications in industrial and research fields, and it is currently the subject of an active research, see [1–8] and therein references. There are numerous methodologies devised to approximate the incompressible linear elasticity equations, including stabilized finite element methods (FEM) [9–13], discontinuous Galerkin methods [14], methods based on the least square approach [15], finite volume methods [1], collocation approaches [16], isogeometric approaches [17–19], and boundary element methods [20].

It is well known that the use of standard finite element approximations (as well as other approaches, see, e.g., [1, 21, 22] and the references therein) in elasticity problems is restricted due to the Poisson locking (dilatation), which is associated with the mathematical formulation being dependent on the Poisson ratio. In the limiting case where the Poisson ratio is equal to 0.5, the unknown of the problem (displacement) is divergence free, whose imposition in the formulation leads to the locking phenomenon (see, for instance [23–26]). As opposed to the application in various structural models involving compressible materials, the incompressible media necessitate the incorporation of the pressure, or mean stress, into the model. In the standard Galerkin formulations, the displacement and pressure interpolations are required to satisfy the classical Babuška–Brezzi inf–sup condition [14, 22, 27–29]. These considerations apply to both the classical boundary value problem defining steady state incompressible elasticity (equivalently incompressible fluid flows) and the eigenproblem to be described in the sequel.

Aiming at avoiding the volumetric locking at the incompressible limit as well as circumventing the restrictions associated with the inf–sup condition, a great number of alter-

*Corresponding author
Email addresses: ramon.codina@upc.edu (Ramon Codina), onder.turk@yandex.com (Önder Türk)

native stabilized finite element approaches have been proposed to solve the incompressible elasticity problems. An analysis of a mixed enhanced strain finite element method for the displacement-pressure formulation is presented in [30]. A mixed finite element method using primal and dual meshes is implemented in [29], where the standard space for the displacement is enriched with element-wise bubble functions. Another mixed formulation based on the dynamic variational multiscale approach is proposed in [31], where the momentum equation is complemented by a rate equation for the evaluation of the pressure. Stabilization strategies based on mesh-free polynomial projection methods are considered in [32, 33]. In [27], a pressure-curl stabilization approach is proposed in which the determination of the pressure stabilization parameter is based on stability concerns, and the curl stabilization parameter is determined on the account of dispersion.

In the case of transient problems, modal analysis constitutes an efficient alternative that is widely implemented to handle vibration problems of elastic materials (see, e.g., [2, 34–36]). In particular, let us cite the recent work [6], where a finite element method with discontinuous pressure basis functions is implemented to study the free vibrations of incompressible rectangular plates.

In this paper, our main objective is to present a modal analysis technique to simulate the linear elastic behavior of incompressible elastic solids where the incompressibility constraint is enforced by incorporating the pressure. The ultimate aim is to extend the robustness and effectiveness of the modal analysis in the mixed finite element framework recently proposed in [37]. In the system of transient elasticity equations consisting of a second order temporal derivative, a harmonic behavior of the displacement is assumed and each mode is considered to be of the form $\boldsymbol{\phi}(\mathbf{x})\mathrm{e}^{\mathrm{i}\omega t}$, where $\boldsymbol{\phi}(\mathbf{x})$ is the vector field of displacement amplitudes associated with the frequency ω. This is substituted into the equilibrium equations where the forcing terms are not considered in the case of free vibrations, yielding an eigenvalue problem (EVP) in which the eigenfunctions are the amplitudes $\boldsymbol{\phi}(\mathbf{x})$, and the eigenvalues are the squares of the frequencies, ω^2. There exists a complete set of eigensolutions corresponding to positive eigenvalues as the elasticity operator is symmetric and positive definite, and hence, and the true solution can be expressed as a series of modes.

An eigenvalue problem has to be handled with a special precaution when it is approximated by using a stabilized finite element method. A residual based stabilization technique may lead to a quadratic EVP even if it is applied to approximate a linear EVP. We have proposed a FEM for the Stokes EVP that preserves the linearity of the continuous problem in [38]. The method is framed within the variational multiscale (VMS) concept, which assumes that the unknown can be split into a finite element component and a subgrid scale that needs to be modeled, and it has been applied to solve stationary boundary value problems in incompressible linear elasticity models in [11–13, 28], for example. The key point is to consider that this subgrid scale is orthogonal, in the L^2-sense, to the finite element component. After approximating it, the result is a problem for the finite element component of the displacement amplitude and the pressure which permits any spatial interpolation. This yields an EVP that is linear, and that can be solved using arbitrary interpolations for the displacement and the pressure. We also remark here the possibility of alternative directions in approximating EVPs. An example is given in a recent study [8] in which two-field and three-field finite element least squares formulations are presented for EVPs associated with linear elasticity.

This paper is organized as follows. In Section 2 we describe the problem to be solved at the continuous level, both the original elastodynamic equations and the modal analysis, and considering both the differential and the weak form of the equations to be solved. The

stabilized finite element approximation we propose is described in Section 3. Section 4 is concerned with the discrete modal analysis description, from which an approximate time integration scheme is presented and analyzed in Section 5. Numerical results are presented in Section 6, and finally conclusions are drawn in Section 7.

2. Statement of the problem

We consider the problem of modeling the vibrations of an *incompressible* linearly elastic body, assuming in particular infinitesimal strains. This initial and boundary value problem is considered to be defined on an open and bounded polyhedral domain $\Omega \subset \mathbb{R}^d\,(d=2,3)$, with boundary $\partial\Omega = \Gamma_{\mathbf{u}} \cup \Gamma_{\mathbf{t}}$, $\Gamma_{\mathbf{u}} \cap \Gamma_{\mathbf{t}} = \emptyset$, and time $t \in [0,T)$. It consists of finding a displacement field $\mathbf{u} : \Omega \times [0,T) \to \mathbb{R}^d$ and a pressure field $p : \Omega \times (0,T) \to \mathbb{R}$ such that

$$\rho\partial_{tt}^2\mathbf{u} - 2\mu\nabla\cdot(\nabla^S\mathbf{u}) + \nabla p = \mathbf{f} \quad \text{in } \Omega,\ t\in(0,T), \tag{1}$$
$$\nabla\cdot\mathbf{u} = 0 \quad \text{in } \Omega,\ t\in(0,T), \tag{2}$$
$$\mathbf{u} = \mathbf{0} \quad \text{on } \Gamma_{\mathbf{u}},\ t\in(0,T), \tag{3}$$
$$\mathbf{n}\cdot(-p\,\mathbf{I} + 2\mu\nabla^S\mathbf{u}) = \mathbf{t} \quad \text{on } \Gamma_{\mathbf{t}},\ t\in(0,T), \tag{4}$$
$$\mathbf{u} = \mathbf{u}_0 \quad \text{in } \Omega,\ t=0, \tag{5}$$
$$\partial_t\mathbf{u} = \mathbf{v}_0 \quad \text{in } \Omega,\ t=0. \tag{6}$$

In these equations, ∇ denotes the standard nabla operator and ∇^S stands for the symmetrical part of the gradient of a vector field. The data of the problem are the force $\mathbf{f}$, the surface traction $\mathbf{t}$, the initial displacement $\mathbf{u}_0(\mathbf{x})$ and the initial velocity $\mathbf{v}_0(\mathbf{x})$. The density ρ and the shear modulus μ are given physical properties. The unit exterior normal to a domain is denoted as $\mathbf{n}$.

To write the weak form of the problem, let $V = \{\mathbf{v} \in H^1(\Omega)^d \mid \mathbf{v} = \mathbf{0} \text{ on } \Gamma_{\mathbf{u}}\}$ and $Q = L^2(\Omega)$ if $\Gamma_{\mathbf{t}} \neq \emptyset$ and $Q = L^2(\Omega)/\mathbb{R}$ if $\Gamma_{\mathbf{t}} = \emptyset$. The inner product in $L^2(\Omega)$ (for scalars, vectors or tensors) is written as $(\cdot,\cdot)$, in $H^1(\Omega)$ as $(\cdot,\cdot)_{H^1}$, and the integral of the product of two functions (for scalars or vectors) in a region R as $\langle\cdot,\cdot\rangle_R$. Assuming $\mathbf{f} : (0,T) \to H^{-1}(\Omega)^d$, $\mathbf{t} : (0,T) \to H^{-1/2}(\Gamma_{\mathbf{t}})^d$, $\mathbf{u}_0 \in V$ and $\mathbf{v}_0 \in L^2(\Omega)^d$, the weak form of Problem (1)-(6) consists of finding $\mathbf{u} : [0,T) \to V$ and $p : (0,T) \to Q$ such that

$$\rho(\partial_{tt}^2\mathbf{u},\mathbf{v}) + 2\mu(\nabla^S\mathbf{u},\nabla^S\mathbf{v}) - (p,\nabla\cdot\mathbf{v}) = \langle\mathbf{f},\mathbf{v}\rangle_\Omega + \langle\mathbf{t},\mathbf{v}\rangle_{\Gamma_{\mathbf{t}}} \quad \forall\mathbf{v}\in V,\ t\in(0,T), \tag{7}$$
$$(q,\nabla\cdot\mathbf{u}) = 0 \quad \forall q\in Q,\ t\in(0,T), \tag{8}$$
$$(\mathbf{u},\mathbf{v})_{H^1} = (\mathbf{u}_0,\mathbf{v})_{H^1} \quad \forall\mathbf{v}\in V,\ t=0, \tag{9}$$
$$(\partial_t\mathbf{u},\mathbf{v}) = (\mathbf{v}_0,\mathbf{v}) \quad \forall\mathbf{v}\in L^2(\Omega)^d,\ t=0. \tag{10}$$

The modal analysis at the continuous level of Problem (1)-(6) consists of expressing the solution in terms of the modes of the solution of the homogeneous problem, i.e., the problem obtained with $\mathbf{f} = \mathbf{0}$ and $\mathbf{t} = \mathbf{0}$:

$$\begin{aligned}
\rho\partial_{tt}^2\mathbf{u}_H - 2\mu\nabla\cdot(\nabla^S\mathbf{u}_H) + \nabla p_H &= \mathbf{0} \quad \text{in } \Omega,\ t\in(0,T),\\
\nabla\cdot\mathbf{u}_H &= 0 \quad \text{in } \Omega,\ t\in(0,T),\\
\mathbf{u}_H &= \mathbf{0} \quad \text{on } \Gamma_{\mathbf{u}},\ t\in(0,T),\\
\mathbf{n}\cdot(-p_H\,\mathbf{I} + 2\mu\nabla^S\mathbf{u}_H) &= \mathbf{0} \quad \text{on } \Gamma_{\mathbf{t}},\ t\in(0,T),\\
\mathbf{u}_H &= \mathbf{u}_0 \quad \text{in } \Omega,\ t=0,\\
\partial_t\mathbf{u}_H &= \mathbf{v}_0 \quad \text{in } \Omega,\ t=0.
\end{aligned}$$

Writing the solution to this problem as

$$\mathbf{u}_H(\mathbf{x},t) = \sum_{n=0}^{\infty} \mathrm{e}^{\mathrm{i}\omega_n t}\boldsymbol{\phi}_n(\mathbf{x}), \quad p_H(\mathbf{x},t) = \sum_{n=0}^{\infty} \mathrm{e}^{\mathrm{i}\omega_n t}\psi_n(\mathbf{x}), \tag{11}$$

and assuming the modes to be linearly independent, it turns out that the amplitudes of the modes $\boldsymbol{\phi}_n(\mathbf{x})$, $\psi_n(\mathbf{x})$ and the frequencies ω_n must be the solution of the EVP:

$$-2\mu\nabla\cdot(\nabla^S\boldsymbol{\phi}_n) + \nabla\psi_n = \rho\,\omega_n^2\boldsymbol{\phi}_n \quad \text{in } \Omega, \tag{12}$$

$$\nabla\cdot\boldsymbol{\phi}_n = 0 \quad \text{in } \Omega, \tag{13}$$

$$\boldsymbol{\phi}_n = \mathbf{0} \quad \text{on } \Gamma_{\mathbf{u}}, \tag{14}$$

$$\mathbf{n}\cdot(-\psi_n\,\mathbf{I} + 2\mu\nabla^S\boldsymbol{\phi}_n) = \mathbf{0} \quad \text{on } \Gamma_{\mathbf{t}}, \tag{15}$$

for $n = 1, 2, \ldots$. It is known that for this problem there is a complete set of eigenfunctions and corresponding eigenvalues which can be arranged as

$$\{\boldsymbol{\phi}_1(\mathbf{x}), \ldots, \boldsymbol{\phi}_n(\mathbf{x}), \ldots\}, \quad \{\psi_1(\mathbf{x}), \ldots, \psi_n(\mathbf{x}), \ldots\}, \quad 0 < \omega_1^2 \leq \omega_2^2 \leq \ldots \omega_n^2 \leq \ldots,$$

which are eigenpairs (non-trivial solutions) of (12)-(15). The displacement eigenfunctions and their symmetric gradients can be taken to be $L^2(\Omega)$-orthogonal, satisfying

$$(\boldsymbol{\phi}_i, \boldsymbol{\phi}_j) = |\Omega|\delta_{ij}, \quad 2\mu(\nabla^S\boldsymbol{\phi}_i, \nabla^S\boldsymbol{\phi}_j) = \rho\,\omega_i^2|\Omega|\delta_{ij}, \quad i,j = 1,2,\ldots, \tag{16}$$

where δ_{ij} is the Kronecker delta. The volume of the computational domain $|\Omega|$ has been introduced to consider the displacement eigenfunctions dimensionless. Thus, these eigenfunctions are indeed linearly independent.

In what follows, we shall omit the subscript n in the eigenfunctions $\boldsymbol{\phi}_n$, ψ_n and eigenvalues ω_n^2, understanding that they correspond to a particular mode of the decomposition in Equation (11). The same will be done for the discrete counterpart of the problem developed in the following section.

The weak form of the EVP (12)-(15) can be written as follows: find $\boldsymbol{\phi} \in V$, $\psi \in Q$ and $\omega^2 \in \mathbb{R}^+$ such that

$$2\mu(\nabla^S\boldsymbol{\phi}, \nabla^S\mathbf{v}) - (\psi, \nabla\cdot\mathbf{v}) = \rho\,\omega^2(\boldsymbol{\phi}, \mathbf{v}) \quad \forall\mathbf{v} \in V, \tag{17}$$

$$(q, \nabla\cdot\boldsymbol{\phi}) = 0 \quad \forall q \in Q. \tag{18}$$

3. Finite element approximation of the eigenproblem

3.1. Galerkin finite element approximation

Let us consider a finite element partition $\mathcal{T}_h = \{K\}$ of the domain Ω, with size $h = \max_{K\in\mathcal{T}_h}\mathrm{diam}(K)$. The collection of all edges of this partition is denoted as $\mathcal{E}_h = \{E\}$. From $\mathcal{T}_h$ we may construct finite element spaces V_h and Q_h to approximate V and Q, respectively. We will restrict in the following to conforming approximations. Likewise, we shall need the space $\bar{V}_h \subset H^1(\Omega)^d$, constructed as V_h but without prescribing the Dirichlet boundary conditions.

Let $n_{\mathbf{u}}$ be the number of nodes to interpolate the displacement and n_p the number of nodes to interpolate the pressure. The finite element approximations to $\mathbf{u}$ and p,

respectively denoted $\mathbf{u}_h$ and p_h, will be

$$\mathbf{u}(\mathbf{x},t) \approx \mathbf{u}_h(\mathbf{x},t) = \sum_{a=1}^{n_{\mathbf{u}}} N^a_{\mathbf{u}}(\mathbf{x})\mathbf{u}^a(t), \quad p(\mathbf{x},t) \approx p_h(\mathbf{x},t) = \sum_{b=1}^{n_p} N^b_p(\mathbf{x})p^b(t), \tag{19}$$

where $N^a_{\mathbf{u}}(\mathbf{x})$ and $N^b_p(\mathbf{x})$ are the displacement and pressure shape functions and $\mathbf{u}^a(t)$ and $p^b(t)$ the displacement and pressure nodal values, respectively. The Galerkin finite element approximation of Problem (7)-(10) consists of finding $\mathbf{u}_h : [0,T) \to V_h$ and $p_h : (0,T) \to Q_h$ such that

$$\rho(\partial^2_{tt}\mathbf{u}_h, \mathbf{v}_h) + 2\mu(\nabla^S\mathbf{u}_h, \nabla^S\mathbf{v}_h) - (p_h, \nabla\cdot\mathbf{v}_h) = \langle \mathbf{f}, \mathbf{v}_h\rangle_\Omega + \langle \mathbf{t}, \mathbf{v}_h\rangle_{\Gamma_{\mathbf{t}}} \quad \forall \mathbf{v}_h \in V_h,\ t \in (0,T), \tag{20}$$

$$(q_h, \nabla\cdot\mathbf{u}_h) = 0 \quad \forall q_h \in Q_h,\ t \in (0,T), \tag{21}$$

$$(\mathbf{u}_h, \mathbf{v}_h)_{H^1} = (\mathbf{u}_0, \mathbf{v}_h)_{H^1} \quad \forall \mathbf{v}_h \in V_h,\ t = 0, \tag{22}$$

$$(\partial_t\mathbf{u}_h, \mathbf{v}_h) = (\mathbf{v}_0, \mathbf{v}_h) \quad \forall \mathbf{v}_h \in V_h,\ t = 0. \tag{23}$$

It is well known that this formulation yields stable displacement-pressure results only if an inf–sup condition is satisfied between the corresponding approximation spaces V_h and Q_h. This restricts significantly the possible choices for these spaces. To avoid this restriction, we propose in the following a stabilized finite element formulation that is stable for any choice of V_h and Q_h. Obviously, these comments for the elastodynamic Problem (7)-(10) are also applicable to the EVP (17)-(18), whose discrete Galerkin finite element version consists of finding $\boldsymbol{\phi}_h \in V_h$, $\psi_h \in Q_h$ and $\omega_h^2 \in \mathbb{R}^+$ such that

$$2\mu(\nabla^S\boldsymbol{\phi}_h, \nabla^S\mathbf{v}_h) - (\psi_h, \nabla\cdot\mathbf{v}_h) = \rho\,\omega_h^2(\boldsymbol{\phi}_h, \mathbf{v}_h) \quad \forall \mathbf{v}_h \in V_h, \tag{24}$$

$$(q_h, \nabla\cdot\boldsymbol{\phi}_h) = 0 \quad \forall q_h \in Q_h. \tag{25}$$

3.2. Stabilized finite element formulation

We propose to use a stabilized finite element method based on the Variational Multi-Scale (VMS) concept. We will not detail the formulation here, which can be found elsewhere [11–13, 39]. This formulation reads: find $\mathbf{u}_h : [0,T) \to V_h$ and $p_h : (0,T) \to Q_h$ such that

$$\begin{aligned}
&\rho(\partial^2_{tt}\mathbf{u}_h, \mathbf{v}_h) + 2\mu(\nabla^S\mathbf{u}_h, \nabla^S\mathbf{v}_h) - (p_h, \nabla\cdot\mathbf{v}_h) \\
&\quad + (q_h, \nabla\cdot\mathbf{u}_h) - \langle \mathbf{f}, \mathbf{v}_h\rangle_\Omega - \langle \mathbf{t}, \mathbf{v}_h\rangle_{\Gamma_{\mathbf{t}}} \\
&\quad + \sum_K \tau_K \left\langle \tilde{P}\left[\rho\partial^2_{tt}\mathbf{u}_h - 2\mu\nabla\cdot(\nabla^S\mathbf{u}_h) + \nabla p_h - \mathbf{f}\right], 2\mu\nabla\cdot(\nabla^S\mathbf{v}_h) + \nabla q_h \right\rangle_K \\
&\quad + \sum_E \tau_E \left\langle [\![-p_h\mathbf{I} + 2\mu\nabla^S\mathbf{u}_h]\!], [\![-q_h\mathbf{I} - 2\mu\nabla^S\mathbf{v}_h]\!] \right\rangle_E = 0,
\end{aligned} \tag{26}$$

for all $\mathbf{v}_h \in V_h$ and $q_h \in Q_h$, and satisfying also the initial conditions (22) and (23). In this equation, $\tilde{P}$ is a projection than can be taken as $\tilde{P} = I$ (the identity) in *classical residual-based stabilized finite element methods* or $\tilde{P} = P_h^\perp$, the $L^2(\Omega)$-projection to the space orthogonal to $\bar{V}_h$ (recall that $V_h \subset \bar{V}_h$, as functions in $\bar{V}_h$ do not necessarily satisfy the Dirichlet boundary conditions). The jump of a tensor $\mathbf{T}$ over an edge is defined as $[\![\mathbf{T}]\!]_E = \mathbf{n}_1\cdot\mathbf{T}|_{\partial K_1\cap E} + \mathbf{n}_2\cdot\mathbf{T}|_{\partial K_2\cap E}$, where K_1 and K_2 are the elements that share the edge E, disregarding the second term if $E \subset \partial\Omega$. Finally, τ_K and τ_E are the stabilization

parameters, computed as

$$\tau_K = \frac{h_K^2}{4\mu k^2}, \quad \tau_E = \frac{h_K}{4\mu k},$$

k being the order of the finite element polynomials. In the following, we will consider the finite element meshes quasi-uniform, so that these parameters can be computed with the diameter of the finite element partition. In the general case, the weighted projections described in [40] can be used.

The formulation given by Equation (26) is quite general. It allows for arbitrary interpolations of displacement and pressure, yielding stable and optimally accurate solutions, in particular when *equal* interpolation is used. However, particular care is needed if we wish to apply it to the EVP (17)-(18). In this case, the stabilized version of Problem (25) is: find $\boldsymbol{\phi}_h \in V_h$, $\psi_h \in Q_h$ and $\omega_h^2 \in \mathbb{R}^+$ such that

$$\begin{aligned} &2\mu(\nabla^S \boldsymbol{\phi}_h, \nabla^S \mathbf{v}_h) - (\psi_h, \nabla \cdot \mathbf{v}_h) + (q_h, \nabla \cdot \boldsymbol{\phi}_h) - \rho\,\omega_h^2(\boldsymbol{\phi}_h, \mathbf{v}_h) \\ &\quad + \sum_K \tau_K \left\langle \tilde{P}\left[-2\mu\nabla\cdot(\nabla^S\boldsymbol{\phi}_h) + \nabla\psi_h - \omega_h^2\boldsymbol{\phi}_h\right], 2\mu\nabla\cdot(\nabla^S\mathbf{v}_h) + \nabla q_h + \omega_h^2\mathbf{v}_h \right\rangle_K \\ &\quad + \sum_E \tau_E \left\langle [\![-\psi_h\mathbf{I} + 2\mu\nabla^S\boldsymbol{\phi}_h]\!], [\![-q_h\mathbf{I} - 2\mu\nabla^S\mathbf{v}_h]\!] \right\rangle_E = 0, \end{aligned} \tag{27}$$

for all $\mathbf{v}_h \in V_h$ and $q_h \in Q_h$. The obvious difficulty with this *standard residual based* approach, in general, is that if $\tilde{P}[\boldsymbol{\phi}_h] \neq \mathbf{0}$ the resulting EVP involves ω_h^2 *and* ω_h^4, thus introducing a nonlinearity that would complicate enormously the problem.

The way to overcome this difficulty is to take $\tilde{P} = P_h^\perp$, since $P_h^\perp[\boldsymbol{\phi}_h] = \mathbf{0}$. This case corresponds to the orthogonal sub-grid scale (OSGS) stabilization method. Moreover, we have that $P_h^\perp(f)$ converges to 0 with h at the optimal order in $L^2(\Omega)$ for any function f smooth enough (recall that $P_h^\perp(f) \in \bar{V}_h^\perp$). Thus, there are terms in problems (26) and (27) that can be deleted without sacrificing accuracy. In particular, the shear terms in the residual and in the test functions can be deleted, and $P_h^\perp[\mathbf{f}]$ can be neglected. Noting that $P_h^\perp[\partial_{tt}^2\mathbf{u}_h] = \mathbf{0}$, and that the jump of the shear terms does not contribute to stability, instead of Problem (26) we consider: find $\mathbf{u}_h : [0,T) \to V_h$ and $p_h : (0,T) \to Q_h$ such that

$$\begin{aligned} &\rho(\partial_{tt}^2\mathbf{u}_h, \mathbf{v}_h) + 2\mu(\nabla^S\mathbf{u}_h, \nabla^S\mathbf{v}_h) - (p_h, \nabla\cdot\mathbf{v}_h) + (q_h, \nabla\cdot\mathbf{u}_h) - \langle\mathbf{f}, \mathbf{v}_h\rangle_\Omega - \langle\mathbf{t}, \mathbf{v}_h\rangle_{\Gamma_\mathbf{t}} \\ &\quad + \sum_K \tau_K \left\langle P_h^\perp\left[\nabla p_h\right], P_h^\perp\left[\nabla q_h\right] \right\rangle_K + \sum_E \tau_E \left\langle [\![p_h\mathbf{I}]\!], [\![q_h\mathbf{I}]\!] \right\rangle_E = 0, \end{aligned} \tag{28}$$

for all $\mathbf{v}_h \in V_h$ and $q_h \in Q_h$, and satisfying also the initial conditions (22) and (23). Note that we have applied $P_h^\perp$ to ∇q_h to highlight the symmetry of the formulation, even if it has no effect for quasi-uniform meshes. Finally, instead of Problem (27) we consider: find $\boldsymbol{\phi}_h \in V_h$, $\psi_h \in Q_h$ and $\omega_h^2 \in \mathbb{R}^+$ such that

$$\begin{aligned} &2\mu(\nabla^S \boldsymbol{\phi}_h, \nabla^S \mathbf{v}_h) - (\psi_h, \nabla \cdot \mathbf{v}_h) + (q_h, \nabla \cdot \boldsymbol{\phi}_h) - \rho\,\omega_h^2(\boldsymbol{\phi}_h, \mathbf{v}_h) \\ &\quad + \sum_K \tau_K \left\langle P_h^\perp\left[\nabla\psi_h\right], P_h^\perp\left[\nabla q_h\right] \right\rangle_K + \sum_E \tau_E \left\langle [\![\psi_h\mathbf{I}]\!], [\![q_h\mathbf{I}]\!] \right\rangle_E = 0, \end{aligned} \tag{29}$$

for all $\mathbf{v}_h \in V_h$ and $q_h \in Q_h$. Note that the last term disappears if Q_h is made of continuous functions.

This is the two-field formulation for the Stokes EVP considered in [38]. It is shown there that it provides stable and optimally accurate eigenfunctions and eigenvalues.

3.3. Algebraic version

Let $U(t)$ be the array that contains the displacement nodal values and $P(t)$ the array that contains the pressure nodal values (see Equation (19)). After imposing the Dirichlet boundary conditions, let $n'_{\mathbf{u}}$ be the size of $U(t)$. Let also U_0 and V_0 be the initial conditions for $U(t)$ and its time derivative, respectively, resulting from equations (22)-(23). Denoting with a dot the time derivative of $U(t)$, the discrete Problem (28) can be written as a differential-algebraic system of equations of the form

$$M\ddot{U} + KU + GP = F, \quad t \in (0,T), \tag{30}$$

$$G^T U - SP = 0, \quad t \in (0,T), \tag{31}$$

$$U = U_0 \quad \text{at } t = 0, \tag{32}$$

$$\dot{U} = V_0 \quad \text{at } t = 0, \tag{33}$$

where $U : [0,T) \to \mathbb{R}^{n'_{\mathbf{u}}}$, $P : [0,T) \to \mathbb{R}^{n_p}$, and with the obvious identification of the matrices and arrays appearing in this expression. With the simplifications introduced, it is observed that matrices M, K and G and the forcing array F are *the same as in the Galerkin approximation*, with $\tau_K = 0$ for all elements $K \in \mathcal{T}_h$ and $\tau_E = 0$ for all edges $E \in \mathcal{E}_h$. The only difference is the appearance of matrix S. In the way we have written Equation (31), *this matrix is symmetric and positive semi-definite*. Obviously, matrices M and K are symmetric and positive definite.

Let $\Phi \in \mathbb{R}^{n'_{\mathbf{u}}}$ be the array of nodal values of displacement amplitudes and $\Psi \in \mathbb{R}^{n_p}$ the array of nodal values of pressure amplitudes. The discrete form of (29) can be written as

$$K\Phi + G\Psi = \omega_h^2 M\Phi, \tag{34}$$

$$G^T\Phi - S\Psi = 0. \tag{35}$$

Since $\text{rank}(M) = n'_{\mathbf{u}}$ (full rank), this system admits $n'_{\mathbf{u}}$ solutions. The discrete eigenvectors and eigenvalues can be written in the form

$$\{\Phi_1, \ldots, \Phi_{n'_{\mathbf{u}}}\}, \quad \{\Psi_1, \ldots, \Psi_{n'_{\mathbf{u}}}\}, \quad 0 < \omega_{h,1}^2 \leq \cdots \leq \omega_{h,n'_{\mathbf{u}}}^2.$$

Let us note here that the pressure eigenfunctions are associated to the displacement ones. A generalized EVP with a positive definite matrix in the right-hand-side multiplying both displacements and pressures would have $n'_{\mathbf{u}} + n_p$ eigenvalues, but there is no term multiplying Ψ in the right-hand-side of Equation (35) (see [41]).

4. Discrete modal analysis

In the previous section we have presented the stabilized finite element formulation we propose to solve the EVP arising in the modal analysis of elastodynamics. Now we derive the expression of the solution of the discrete elastodynamic Problem (30)-(33) in terms of the eigenvalues and eigenfunctions obtained from Problem (34)-(35). The expression to be obtained is exact; we defer to the following section the truncation of this solution and the analysis of the underlying error.

We will prove that the solution to (30)-(33) can be written as

$$\begin{bmatrix} U(t) \\ P(t) \end{bmatrix} = \sum_{j=1}^{n'_{\mathbf{u}}} z_j(t) \begin{bmatrix} \Phi_j \\ \Psi_j \end{bmatrix}, \tag{36}$$

with appropriate scalar functions $z_j(t)$ to be determined, $j = 1, \ldots, n'_{\mathbf{u}}$. The proof is constructive, obtaining effectively the expression of these functions. In particular, it is observed that the time evolution of the displacement modes is the same as that of the pressure modes. The derivation will follow standard steps, although it will serve to highlight the role played by the stabilization term represented by matrix S. Let

$$\Xi = \begin{bmatrix} \Phi_1 \cdots \Phi_{n'_{\mathbf{u}}} \\ \Psi_1 \cdots \Psi_{n'_{\mathbf{u}}} \end{bmatrix} \in \mathbb{R}^{(n'_{\mathbf{u}}+n_p)\times n'_{\mathbf{u}}}, \quad Z(t) = \begin{bmatrix} z_1(t) \\ \vdots \\ z_{n'_{\mathbf{u}}}(t) \end{bmatrix} \in \mathbb{R}^{n'_{\mathbf{u}}}, \tag{37}$$

which allow us to write

$$\begin{bmatrix} U(t) \\ P(t) \end{bmatrix} = \Xi Z(t). \tag{38}$$

Substituting this into (30)-(31), and multiplying by the left by Ξ^T we get

$$\Xi^T \begin{bmatrix} M & 0 \\ 0 & 0 \end{bmatrix} \Xi \ddot{Z}(t) + \Xi^T \begin{bmatrix} K & G \\ G^T & -S \end{bmatrix} \Xi Z(t) = \Xi^T \begin{bmatrix} F \\ 0 \end{bmatrix}. \tag{39}$$

In expanded form, we have

$$\Phi_i^T \sum_{j=1}^{n'_{\mathbf{u}}} M\Phi_j \ddot{z}_j + \Phi_i^T \sum_{j=1}^{n'_{\mathbf{u}}} \left(K\Phi_j + G\Psi_j\right) z_j = \Phi_i^T F, \quad i = 1, \ldots, n'_{\mathbf{u}}, \tag{40}$$

$$\Psi_i^T \sum_{j=1}^{n'_{\mathbf{u}}} \left(G^T\Phi_j - S\Psi_j\right) z_j = 0, \quad i = 1, \ldots, n'_{\mathbf{u}}. \tag{41}$$

The discrete counterpart of the $L^2(\Omega)$-orthogonality in (16) translates into:

$$\Phi_i^T M \Phi_j = m\delta_{ij}, \quad i, j = 1, \ldots, n'_{\mathbf{u}}, \tag{42}$$

where $m = \rho|\Omega|$ is a scalar with the units of M (mass, in our case). Therefore, from (34) we get

$$\Phi_i^T \left(K\Phi_j + G\Psi_j\right) = \omega_{h,j}^2 m\delta_{ij}. \tag{43}$$

From (35) we have that (41) is automatically satisfied. Setting $f_i := m^{-1}\Phi_i^T F$, from (40) we obtain

$$\ddot{z}_i + \omega_{h,i}^2 z_i = f_i, \quad i = 1, \ldots, n'_{\mathbf{u}}. \tag{44}$$

It is important to remark that the equations obtained are the same as for the non-incompressible case using a displacement formulation and as for the Galerkin approximation to the incompressible case. For the Galerkin case ($S = 0$), we would have $\Phi_i^T G\Psi_j = 0$, but in fact what we need is (43), which also holds in the stabilized case. Also note that expansion (36) has to be assumed in the method we have employed; however, one could in principle use different expressions of z for the displacement and pressure in the Galerkin case. Nevertheless, as the solution is unique, this is the one we will find.

The solution of the differential equation (44) can be written as

$$z_i(t) = z_{i,H}(t) + z_{i,P}(t), \quad i = 1, \ldots, n'_{\mathbf{u}}, \tag{45}$$

where $z_{i,H}(t)$ is the general solution of the corresponding homogeneous equation, and $z_{i,P}(t)$ is a particular solution. Note that in the case in which f_i is independent of time, the particular solution can be taken in the form $z_{i,P} = \omega_{h,i}^{-2} f_i, i = 1, \ldots, n'_{\mathbf{u}}$.

Consequently, the solution of the non-homogeneous Problem (30)-(33) becomes

$$\begin{bmatrix} U(t) \\ P(t) \end{bmatrix} = \sum_{j=1}^{n'_{\mathbf{u}}} (A_j \mathrm{e}^{\mathrm{i}\omega_{h,j}t} + B_j \mathrm{e}^{-\mathrm{i}\omega_{h,j}t} + z_{j,P}(t)) \begin{bmatrix} \Phi_j \\ \Psi_j \end{bmatrix}, \tag{46}$$

where A_j, B_j, $j = 1, \ldots, n'_{\mathbf{u}}$, are the coefficients to be determined from the initial conditions projected onto the subspace generated by the modes:

$$U(0) = \sum_{j=1}^{n'_{\mathbf{u}}} (A_j + B_j + z_{j,P}(0))\Phi_j = \sum_{j=1}^{n'_{\mathbf{u}}} \frac{1}{m} (\Phi_j^T M U_0)\Phi_j, \tag{47}$$

$$\dot{U}(0) = \sum_{j=1}^{n'_{\mathbf{u}}} (\mathrm{i}\omega_{h,j} A_j - \mathrm{i}\omega_{h,j} B_j + \dot{z}_{j,P}(0))\Phi_j = \sum_{j=1}^{n'_{\mathbf{u}}} \frac{1}{m} (\Phi_j^T M V_0)\Phi_j, \tag{48}$$

from which we arrive at the following relations

$$A_j + B_j + z_{j,P}(0) = \frac{1}{m}\Phi_j^T M U_0, \quad \mathrm{i}\omega_{h,j} A_j - \mathrm{i}\omega_{h,j} B_j + \dot{z}_{j,P}(0) = \frac{1}{m}\Phi_j^T M V_0, \tag{49}$$

for $j = 1, \ldots, n'_{\mathbf{u}}$. It is trivially checked that the solution for A_j, B_j is unique, thus proving that the solution of Problem (30)-(33) can be written as indicated in Equation (36).

As a summary, the results obtained are analogous to those known for the irreducible displacement formulation in the case of compressible elastic solids. Here he have extended them to the incompressible case using a displacement-pressure formulation and a stabilized finite element method.

5. Truncated solution and error analysis

The term *modal analysis* often refers to the *approximate* method in which only a few modes of expansion (36) are kept, that is to say, the solution is approximated as

$$U(t) = \sum_{i=1}^{n'_{\mathbf{u}}} z_i(t)\Phi_i \approx U_{m_{\mathbf{u}}}(t) = \sum_{i=1}^{m_{\mathbf{u}}} z_i(t)\Phi_i, \tag{50}$$

$$P(t) = \sum_{i=1}^{n'_{\mathbf{u}}} z_i(t)\Psi_i \approx P_{m_{\mathbf{u}}}(t) = \sum_{i=1}^{m_{\mathbf{u}}} z_i(t)\Psi_i, \tag{51}$$

with $m_{\mathbf{u}} \leq n'_{\mathbf{u}}$ (in the applications, $m_{\mathbf{u}} \ll n'_{\mathbf{u}}$). The concern now is to bound the error associated to this approximation, and in particular to measure the difference $U(t) - U_{m_{\mathbf{u}}}(t)$. This will be done with norms associated to matrices.

Let A be a $n \times n$ symmetric and *positive definite* matrix, and X, Y arrays of size n.

We define the norms:

$$\|X\|_A := (X^T A X)^{1/2}, \quad \|Y\|_{-A} := \sup_{X \neq 0} \frac{X^T Y}{\|X\|_A}.$$

It is assumed in the second expression that the product $X^T Y$ makes sense; in particular, the units of the components of X and Y make $X^T Y$ dimensionally meaningful. Note also that the Schwarz-type inequality $X^T Y \leq \|X\|_A \|Y\|_{-A}$ is easily checked. If A is only positive semi-definite, $\|X\|_A$ is a semi-norm rather than a norm.

In our problem, when $A = M$ we have that $\|X\|_A$ is the $L^2(\Omega)$ norm of the finite element function with nodal values X (multiplied by ρ) and when $A = K$ it is equivalent to the $H^1(\Omega)$ seminorm of this function (multiplied by μ). When $A = S$, $\|X\|_S$ is a semi-norm.

We will obtain an estimate for $\|U - U_{m_{\mathbf{u}}}\|_M$, that is to say, an $L^2(\Omega)$ error estimate for the displacement error when approximation (50) is used. Let us start noting that, because of the $L^2(\Omega)$-orthogonality of the displacement modes, we have

$$\begin{aligned} \|U\|_M^2 &= \sum_{i,j=1}^{n'_{\mathbf{u}}} z_i z_j \Phi_i^T M \Phi_j = \sum_{i=1}^{n'_{\mathbf{u}}} z_i^2 m, \\ \|U - U_{m_{\mathbf{u}}}\|_M^2 &= \sum_{i,j=m+1}^{n'_{\mathbf{u}}} z_i z_j \Phi_i^T M \Phi_j = \sum_{i=m+1}^{n'_{\mathbf{u}}} z_i^2 m. \end{aligned} \tag{52}$$

Let us evaluate now the following norm:

$$\begin{aligned} \|U\|_K^2 + \|P\|_S^2 &= \sum_{i,j=1}^{n'_{\mathbf{u}}} z_i z_j \Phi_i^T K \Phi_j + \sum_{i,j=1}^{n'_{\mathbf{u}}} z_i z_j \Psi_i^T S \Psi_j \\ &= \sum_{i,j=1}^{n'_{\mathbf{u}}} z_i z_j \Phi_i^T K \Phi_j + \sum_{i,j=1}^{n'_{\mathbf{u}}} z_i z_j \Psi_i^T G^T \Phi_j \quad \text{(using (35))} \\ &= \sum_{i,j=1}^{n'_{\mathbf{u}}} z_i z_j \Phi_j^T (K \Phi_i + G \Psi_i) \\ &= \sum_{i=1}^{n'_{\mathbf{u}}} z_i^2 \omega_{h,i}^2 m \qquad \text{(using (43))}. \end{aligned} \tag{53}$$

The error measure in Equation (52) can be bounded as follows:

$$\begin{aligned}
\|U - U_{m_{\mathbf{u}}}\|_M^2 &= \sum_{i=m_{\mathbf{u}}+1}^{n'_{\mathbf{u}}} z_i^2 m \\
&\leq \frac{1}{\omega_{h,m_{\mathbf{u}}+1}^2} \sum_{i=m_{\mathbf{u}}+1}^{n'_{\mathbf{u}}} \omega_{h,i}^2 z_i^2 m \quad (\text{since } \omega_{h,m_{\mathbf{u}}+1}^2 \leq \omega_{h,i}^2 \text{ for } i \geq m_{\mathbf{u}}+1) \\
&\leq \frac{1}{\omega_{h,m_{\mathbf{u}}+1}^2} \sum_{i=1}^{n'_{\mathbf{u}}} \omega_{h,i}^2 z_i^2 m \\
&= \frac{1}{\omega_{h,m_{\mathbf{u}}+1}^2} \left(\|U\|_K^2 + \|P\|_S^2 \right) \quad (\text{using (53)}). \qquad (54)
\end{aligned}$$

This is in fact the result we were seeking. If we prove that $\|U\|_K^2 + \|P\|_S^2$ is bounded, that is to say, the solution is stable in this norm, then the bound obtained establishes that the $L^2(\Omega)$ norm of the error in displacements is of the order of the inverse of the frequency of the first term disregarded in approximation (50).

It remains therefore to obtain a stability estimate for $\|U\|_K^2 + \|P\|_S^2$. Multiplying Equation (30) by $\dot{U}^T$ we get:

$$\dot{U}^T M \ddot{U} + \dot{U}^T K U + \dot{U}^T G P = \dot{U}^T F. \qquad (55)$$

From Equation (31) differentiated with respect to time we obtain:

$$\dot{U}^T G P = P^T G^T \dot{U} = P^T S \dot{P}. \qquad (56)$$

Taking into account the symmetry of M, K and S, Equations (55) and (56) yield:

$$\frac{1}{2}\frac{\mathrm{d}}{\mathrm{d}t}\|\dot{U}\|_M^2 + \frac{1}{2}\frac{\mathrm{d}}{\mathrm{d}t}\|U\|_K^2 + \frac{1}{2}\frac{\mathrm{d}}{\mathrm{d}t}\|P\|_S^2 = \dot{U}^T F. \qquad (57)$$

To obtain a bound from this expression, we will use the fact that the solution to Problem (30)-(33) can be split as $U = U_I + U_F$, $P = P_I + P_F$, where subscript I refers to the problem with zero forcing term but non-zero initial conditions and subscript F to the problem with zero initial conditions and non-zero forcing term.

Since the initial pressure is not required, we may take it zero. Integrating Equation (57) with respect to time up to an arbitrary $t_0 \in (0, T)$ for the problem with $F = 0$ we obtain:

$$\|\dot{U}_I(t_0)\|_M^2 + \|U_I(t_0)\|_K^2 + \|P_I(t_0)\|_S^2 = \|V_0\|_M^2 + \|U_0\|_K^2,$$

from where

$$\max_{t\in(0,T)} \|U_I(t)\|_K^2 + \max_{t\in(0,T)} \|P_I(t)\|_S^2 \leq \|V_0\|_M^2 + \|U_0\|_K^2. \qquad (58)$$

For the case with homogeneous initial conditions and $F \neq 0$, from Schwarz' inequality and Young's inequality we obtain:

$$\dot{U}_F^T F \leq \|\dot{U}_F\|_M \|F\|_{-M} \leq \frac{1}{2s}\|\dot{U}_F\|_M^2 + \frac{s}{2}\|F\|_{-M}^2,$$

for any time $s \in (0,T)$. Using this in (57) and integrating up to any $t_0 \in (0,T)$, it follows that

$$\|\dot{U}_F(t_0)\|_M^2 + \|U_F(t_0)\|_K^2 + \|P_F(t_0)\|_S^2 \leq \int_0^{t_0} \frac{1}{s}\|\dot{U}_F(s)\|_M^2 \mathrm{d}s + \int_0^{t_0} s\|F(s)\|_{-M}^2 \mathrm{d}s. \quad (59)$$

Now we need a boundedness assumption for F. For example, assuming that

$$\|F\|_T^2 := \max_{t\in(0,T)} t \int_0^t \frac{1}{s^2}\left[\int_0^s r\|F(r)\|_{-M}^2 \mathrm{d}r\right] \mathrm{d}s < \infty,$$

using Gronwall's Lemma it follows from (59) that

$$\max_{t\in(0,T)} \|U_F(t)\|_K^2 + \max_{t\in(0,T)} \|P_F(t)\|_S^2 \leq \|F\|_T^2. \quad (60)$$

The triangle inequality combined with estimates (58) and (60) allows us to conclude that

$$\max_{t\in(0,T)} \|U(t)\|_K^2 + \max_{t\in(0,T)} \|P(t)\|_S^2 \leq \|V_0\|_M^2 + \|U_0\|_K^2 + \|F\|_T^2.$$

Finally, using this stability estimate in the error estimate (54) we obtain

$$\max_{t\in(0,T)} \|U(t) - U_{m_{\mathbf{u}}}(t)\|_M \lesssim \frac{1}{\omega_{m_{\mathbf{u}}+1}} \left(\|V_0\|_M + \|U_0\|_K + \|F\|_T\right), \quad (61)$$

where $\lesssim$ stands for $\leq$ up to constants. This is the error estimate we wished to prove. Again, it is analogous to what would be obtained for the irreducible displacement formulation for compressible materials. Apart from the novel proof, we have extended it to incompressible elasticity using the displacement-pressure formulation, highlighting the role played by the stabilization term given by matrix S.

6. Numerical results

We present our numerical results on incompressible linear elasticity equations that confirm the theoretical analysis of the formulation proposed in this work. We focus ourselves on two different setups of plane stress problems, namely a rectangular cantilever beam and the well known Cook's membrane problem are considered. We have chosen these examples because $F = 0$, $U_0 \neq 0$ for the cantilever beam and $F \neq 0$, $U_0 = 0$ for Cook's membrane.

In the numerical experiments, we use quadratic type triangular elements having six nodes located at the vertices and on the midpoints of the edges to discretize each problem domain, and employ the method with equal order interpolations for both the displacement field and the pressure. The number of divisions in the horizontal and vertical directions are denoted by N_x and N_y, respectively.

In order to be able to evaluate the results we obtain from the truncation of the sums given in Equations (50)-(51), we approximate the solution of Problem (30)-(33) by directly integrating in time with the use of a backward differentiation formula. This is a four–point backward difference approximation to the second order time derivative which is second order accurate, and is given for a time step δt on a discrete set of time instants $t_i = i\delta t$, $i = 3, 4, \ldots, N_T$ in the interval $[0, T]$, as

$$\ddot{U}(t_i) \approx \left(-U(t_{i-3}) + 4U(t_{i-2}) - 5U(t_{i-1}) + 2U(t_i)\right)/\delta t^2 . \quad (62)$$

In what follows, we refer to this formula as the finite difference (FD) time integration scheme.

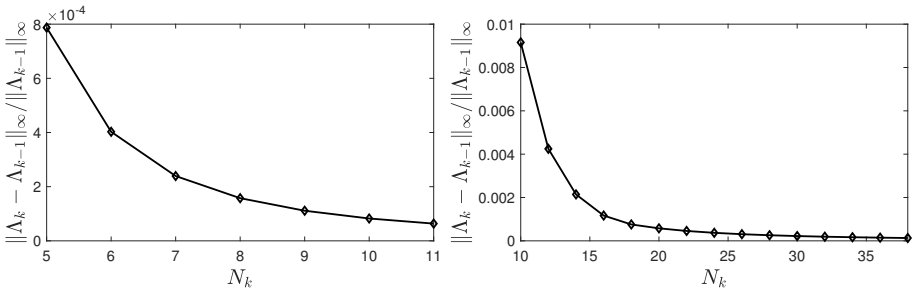

Figure 1: Mesh tests for the cantilever beam problem (left) and Cook's membrane problem (right).

We have performed all the numerical simulations by means of computer programs written by us using MATLAB and exploiting its linear system and generalized matrix eigenvalue problem solvers. In computing the modal expansion of the solutions, we depend on the accuracy of the approximated eigensolutions. As already mentioned, it has been established in [38] that the discrete eigensolutions convergence optimally to their continuous counterparts. Consequently, to determine the number of elements used in the simulations, for each problem we have carried out a mesh test in which we have examined the maximum relative change in the first 10 frequencies contributing into expansion (46) between two successive mesh levels. We have examined the variation of this quantity in terms of the vector infinity norm, that is, $\|\Lambda_k - \Lambda_{k-1}\|_\infty / \|\Lambda_{k-1}\|_\infty$, where Λ_k denotes the array of the first 10 frequencies, $\omega_{h,j}, j = 1, 2, \ldots, 10$, for each discretization level N_k. In the cantilever beam domain we have taken $N_y = N_k$ being varied from 5 to 11, with $N_x = 10N_k$ so as to have a uniform mesh, whereas for Cook's membrane problem we have considered $N_x = N_y = N_k$ and let N_k vary from 8 to 38 with an increment of 2. The results are shown in Figure 1, from which we have concluded that a sufficiently good convergence is attained (specifically, with a tolerance of 10^{-4}) when $N_y = 10$ for the cantilever beam and $N_y = 36$ for Cook's membrane problems. We also list the corresponding first ten approximate frequencies obtained using the aforementioned discretization levels for each problem in Table 1. Consequently, we have used these discretization levels in all the subsequent computations whose results are presented in the following.

Table 1: The first ten frequency approximations for both of the problems.

Cantilever beam	Cook's membrane
0.6420	2.2087
3.7900	5.3987
9.7946	6.8903
10.0443	10.6672
17.4510	13.3620
26.1549	14.7368
29.8846	17.0423
35.4818	18.5002
45.1756	19.5551
48.9939	20.8546

6.1. Free vibration of a cantilever beam

Firstly, we analyze the free vibration of a rectangular beam clamped at the left vertical edge and free at the other vertical side. We take $\rho = 1$ and $\mu = 10^3$, omitting the units, in Equation (1). The beam is assumed to undergo a sudden deflection as a response to an initial load, and then allowed to vibrate harmonically. At the left vertical wall the homogeneous Dirichlet boundary condition is imposed, whereas the other walls are assumed to be free. Thus, the bending is initiated through the initial condition of the displacement, and the initial velocity is assumed to be zero. Figure 2 depicts the initial configuration of the model (where $N_y = 10$), in which the displacements are magnified 50 times to display the primary deformation.

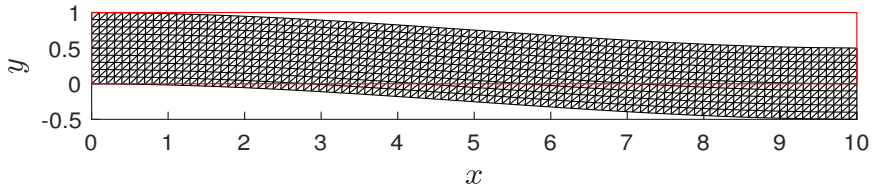

Figure 2: The initial setting of the cantilever beam problem (the displacements are magnified 50 times) where $N_x = 100$ and $N_y = 10$.

As a prelude to analyze the cantilever problem we provide the structures of the first eight eigenmodes that are associated to the displacement field on the finite element mesh in Figure 3. As the problem is governed by the classical equilibrium equations of the incompressible beam, the modes associated to the highest natural frequencies are simple- and multiple-bending modes due to the bending associated with the initial deflection. The eigenstructure contains also pure compression or decompression modes (e.g., Φ_4 and Φ_7). On the other hand, the solution profile is not affected to a large extent with the introduction of these modes as can easily be deduced from the convergence history depicted in Figure 4.

Both to investigate the mechanism of the effect of introducing a new mode into the modal expansion and to verify the convergence analysis given in the previous section, we compute the error $\|U - U_{m_{\mathbf{u}}}\|_M$ using a reference solution obtained using 100 modes, normalized using $\|U\|_K$, and depict its variation with the corresponding eigenvalue $\lambda_{m_{\mathbf{u}}+1}$, for $m_{\mathbf{u}} \leq 60$, in Figure 4. This figure presents the evolution of the error given at a certain time level $t = 5$ where the vertical displacement attains a local maximum (see Figure 5); in any case, all the time levels we explored yield analogous results, which we have not included for conciseness.

In Figure 5 we depict the time evolution of the vertical displacement at the tracking point (the upper right tip of the beam) in the interval $[0, 20]$ computed from three different scenarios: the direct time integration using (62), the modal expansion solution using 8 modes, and the modal expansion solution using 100 modes. The figure shows the reasonably good agreement of the three approximations.

6.2. Cook's membrane problem

We consider a dynamic version of Cook's membrane problem, which is a widely used benchmark test (see, e.g., [4, 31, 42]) to put to the proof the efficiency of the numerical procedure we have proposed. The problem is defined on a quadrilateral domain with corner coordinates given by $(0, 0)$, $(4.8, 4.4)$, $(4.8, 6)$, and $(0, 4.4)$. The discretization of this domain ($N_x = N_y = 36$) is given in Figure 6. The linear elastic model is taken into account,

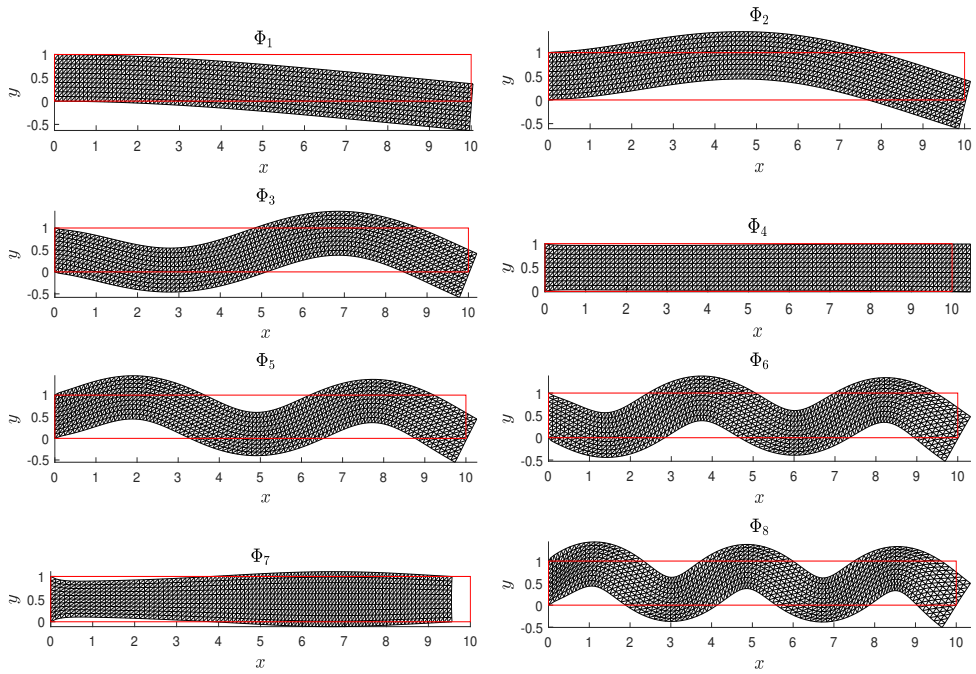

Figure 3: Cantilever beam: The first eight eigenmodes.

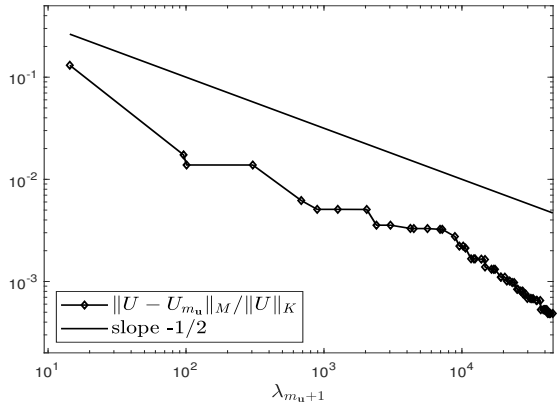

Figure 4: Cantilever beam: Variation of the error with respect to the eigenvalues at $t = 5$.

where the material is assumed to be incompressible with a normalized density (omitting the units) $\rho = 1$, and Young's modulus $E = 250$ ($E = 3\mu$ for incompressible materials). The left vertical edge of the membrane is clamped and therefore zero Dirichlet boundary conditions are imposed for the displacement at that side. The membrane is subjected to a uniform vertical shearing load at the vertical right edge, so that $\mathbf{t} = (0, 6.25)$. Both of the other two edges are assumed to be traction free. Homogeneous initial conditions are considered for the displacement, velocity, and pressure fields and hence the solution is expected to oscillate about the static equilibrium state.

To begin with, as in the previous case we display the displacement field plots associated with the first eight modes on the finite element mesh of Cook's membrane problem in Figure 7. In this bending dominated problem where an additional constant traction exists at the right wall, the characteristics of the computed solutions reflect the mechanics of the membrane and the associated structures; each mode listed in this figure has a meaningful

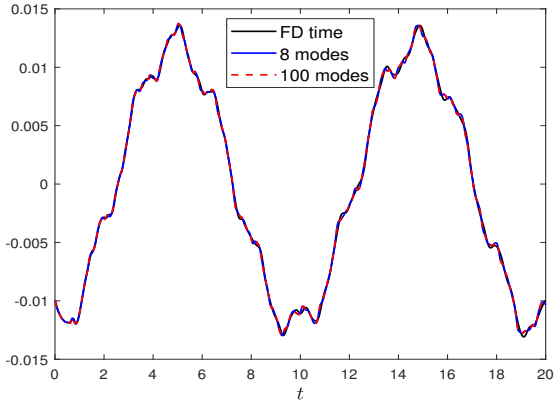

Figure 5: Cantilever beam: Transient behavior of the vertical displacement at the tracking point.

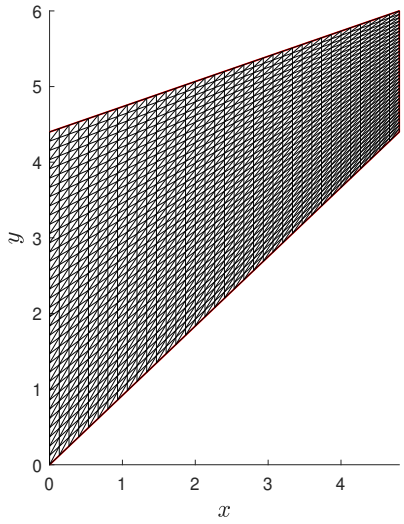

Figure 6: Discretization of Cook's membrane problem domain when $N_x = N_y = 36$.

contribution on the solution profile as can be deduced from the convergence history given in Figure 8.

As has been done for the cantilever beam problem, we investigate the convergence behavior at a certain time ($t = 1.5$) in Figure 8, where we depict the variation of the normalized error between the computed solution with inclusion of the $m_{\mathbf{u}}$-th mode, with $m_{\mathbf{u}} \leq 60$, and a reference solution which is computed using 100 modes in expansion (36) with respect to the corresponding eigenvalue, $\lambda_{m_{\mathbf{u}}+1}$. It can easily be seen from this figure that the error validates the bound given in (61). As anticipated, it is also observed from this figure that including certain modes (e.g., $m_{\mathbf{u}} = 10$ and 11) leads to a slight decrease in the error not having a notable effect on the overall solution structure at the given time for the present configuration.

In Figure 9, we depict the temporal evolution of the displacement by monitoring the vertical displacement at the tracking point (the upper right tip of the membrane) in the interval $[0, 5.5]$ computed with three different schemes: the FD approximation using (62), and the two modal expansion solutions using 8 and 100 modes. It is quite clear from this figure as well that the transient behavior of the membrane can be well captured with a relatively small number of combinations of the displacement modes.

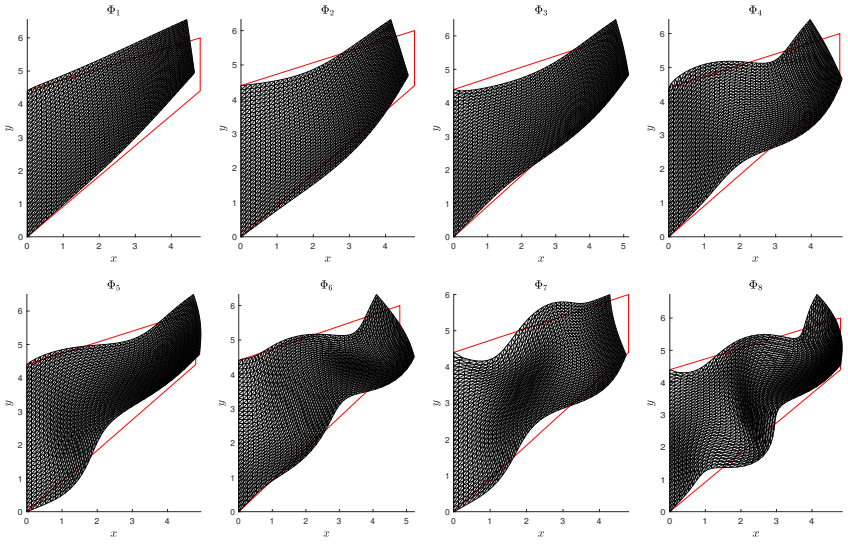

Figure 7: Cook's membrane problem: The first eight eigenmodes.

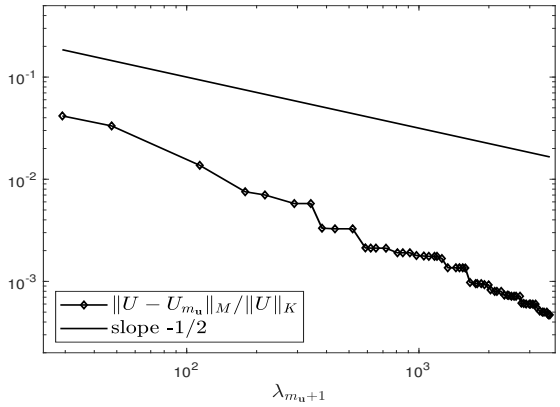

Figure 8: Cook's membrane problem: Variation of the error with respect to the eigenvalues at $t = 1.5$.

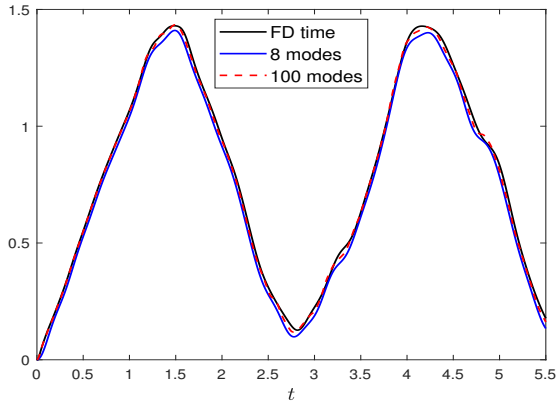

Figure 9: Cook's membrane problem: Transient behavior of the vertical displacement at the tracking point.

Finally, to allow further comparison of the physical aspects of the solutions obtained, we provide in Figure 10 the contour plots of the nodal magnitude distribution of the

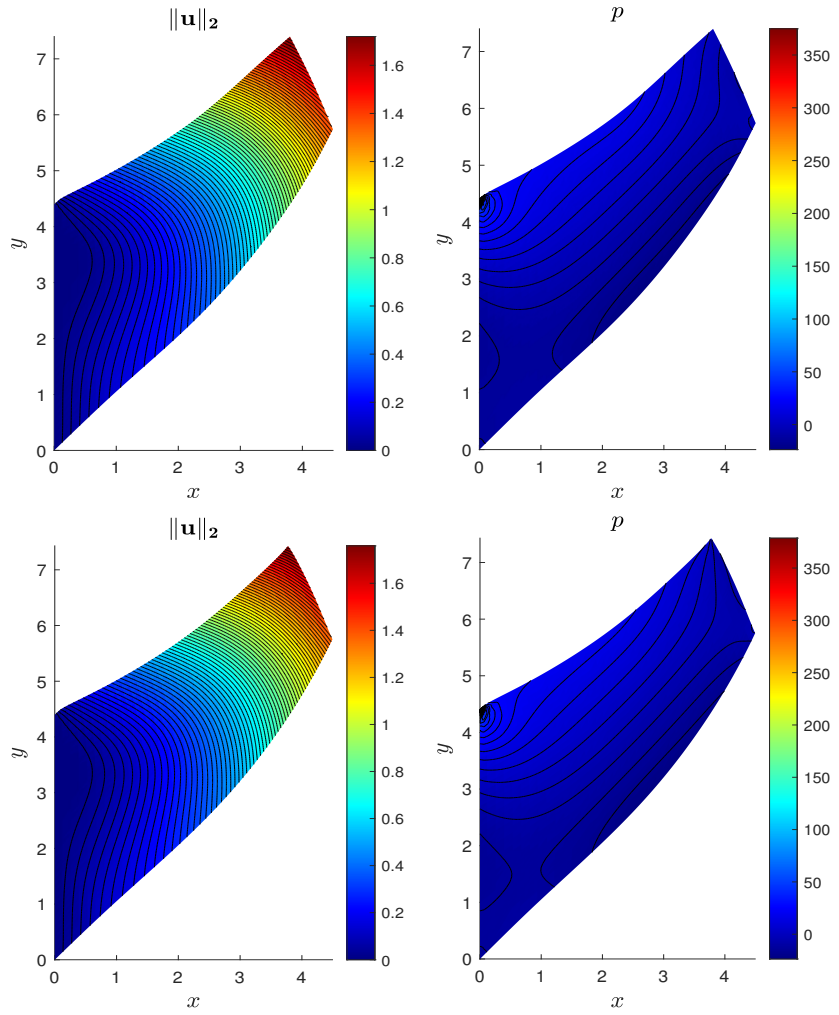

Figure 10: Cook's membrane problem: Nodal displacement magnitude and pressure field at $t = 1.5$; 8-mode (top) and FD in time (bottom) solutions.

displacement and the pressure field on the deformed membrane obtained using both the modal approach with 8 modes and the FD time marching scheme. These results lead us to infer that the solution characteristics obtained from two different approaches are in well agreement, and hence to conclude that the incompressible elasticity model considered can be effectively handled by the modal approach.

7. Conclusion

In this paper we have analyzed the modal analysis technique applied to elastic vibrations of incompressible materials. Incompressibility requires the introduction of pressure as a variable, so we have considered the displacement-pressure formulation. For the spatial approximation of the problem we have adopted a finite element method and, instead of adhering to the inf–sup condition between displacements and pressure to guarantee stability, we have presented a stabilized finite element formulation. It has been highlighted that standard residual based approaches are inappropriate for the associated eigenvalue problem, as they would convert it into a quadratic problem for the eigenvalue (the square of the frequency). We have proposed a method that only involves the pressure in the stabilization

terms, particularly suited for the problem at hand, stable and optimally convergent.

The algebraic version of the differential-algebraic system resulting from the space approximation has then been studied, describing the modal analysis and obtaining an error estimate when the representation of the solution in terms of the modes is truncated. Both this modal analysis and the error of the truncated solution are analogous to those that would be obtained for the irreducible formulation of compressible elastic bodies. However, in the developments presented the pressure and its stabilization play a crucial role. Likewise, a novel purely algebraic approach has been employed in this analysis.

Finally, the numerical results have confirmed that the methodology studied can be effectively used as a time integration scheme to approximate the vibrations of elastic incompressible bodies.

Acknowledgement

R. Codina gratefully acknowledges the support received through the ICREA Academia Research Program of the Catalan Government.

References

[1] I. Bijelonja, I. Demirdi, S. Muzaferija, A finite volume method for incompressible linear elasticity, Computer Methods in Applied Mechanics and Engineering 195 (44) (2006) 6378–6390.

[2] R. Batra, S. Aimmanee, Vibration of an incompressible isotropic linear elastic rectangular plate with a higher-order shear and normal deformable theory, Journal of Sound and Vibration 307 (3) (2007) 961–971.

[3] S. Federico, A. Grillo, S. Imatani, The linear elasticity tensor of incompressible materials, Mathematics and Mechanics of Solids 20 (6) (2015) 643–662.

[4] S. Rossi, N. Abboud, G. Scovazzi, Implicit finite incompressible elastodynamics with linear finite elements: A stabilized method in rate form, Computer Methods in Applied Mechanics and Engineering 311 (2016) 208–249.

[5] N. Viebahn, K. Steeger, J. Schrder, A simple and efficient Hellinger-Reissner type mixed finite element for nearly incompressible elasticity, Computer Methods in Applied Mechanics and Engineering 340 (2018) 278–295.

[6] L. Yuan, R. C. Batra, Vibrations of an incompressible linearly elastic plate using discontinuous finite element basis functions for pressure, Journal of Vibration and Acoustics 141 (5) (2019) 051016.

[7] F. Bertrand, B. Kober, M. Moldenhauer, G. Starke, Weakly symmetric stress equilibration and a posteriori error estimation for linear elasticity, Numerical Methods for Partial Differential Equations 37 (4) (2021) 2783–2802.

[8] F. Bertrand, D. Boffi, Least-squares formulations for eigenvalue problems associated with linear elasticity, Computers & Mathematics with Applications 95 (2021) 19–27.

[9] T. Hughes, L. Franca, M. Balestra, A new finite element formulation for computational fluid dynamics: V. Circumventing the Babuška-Brezzi condition: a stable Petrov-Galerkin formulation for the Stokes problem accommodating equal-order interpolations, Computer Methods in Applied Mechanics and Engineering 59 (1986) 85–99.

[10] L. Franca, T. Hughes, A. Loula, I. Miranda, A new family of stable elements for nearly incompressible elasticity based on a mixed Petrov-Galerkin finite element formulation, Numerische Mathematik 53 (1988) 123–141.

[11] R. Codina, J. Blasco, A finite element formulation for the Stokes problem allowing equal velocity-pressure interpolation, Computer Methods in Applied Mechanics and Engineering 143 (1997) 373–391.

[12] R. Codina, Stabilization of incompressibility and convection through orthogonal subscales in finite element methods, Computer Methods in Applied Mechanics and Engineering 190 (2000) 1579–1599.

[13] R. Codina, J. Principe, J. Baiges, Subscales on the element boundaries in the variational two-scale finite element method, Computer Methods in Applied Mechanics and Engineering 198 (2009) 838–852.

[14] P. Hansbo, M. G. Larson, Discontinuous Galerkin methods for incompressible and nearly incompressible elasticity by Nitsche's method, Computer Methods in Applied Mechanics and Engineering 191 (17) (2002) 1895 – 1908.

[15] Z. Cai, G. Starke, Least-squares methods for linear elasticity, SIAM Journal on Numerical Analysis 42 (2) (2004) 826–842.

[16] S.-W. Chi, J.-S. Chen, H.-Y. Hu, A weighted collocation on the strong form with mixed radial basis approximations for incompressible linear elasticity, Computational Mechanics 53 (2) (2014) 309–324.

[17] F. Auricchio, L. B. da Veiga, A. Buffa, C. Lovadina, A. Reali, G. Sangalli, A fully locking-free isogeometric approach for plane linear elasticity problems: A stream function formulation, Computer Methods in Applied Mechanics and Engineering 197 (1) (2007) 160–172.

[18] L. Beiro da Veiga, D. Cho, L. Pavarino, S. Scacchi, Isogeometric Schwarz preconditioners for linear elasticity systems, Computer Methods in Applied Mechanics and Engineering 253 (2013) 439–454.

[19] D. Cho, L. Pavarino, S. Scacchi, Overlapping additive Schwarz preconditioners for isogeometric collocation discretizations of linear elasticity, Computers & Mathematics with Applications 93 (2021) 66–77.

[20] D. Polyzos, S. Tsinopoulos, D. Beskos, Static and dynamic boundary element analysis in incompressible linear elasticity, European Journal of Mechanics - A/Solids 17 (3) (1998) 515–536.

[21] J. Dolbow, T. Belytschko, Volumetric locking in the element free Galerkin method, International Journal for Numerical Methods in Engineering 46 (6) (1999) 925–942.

[22] D. Boffi, R. Stenberg, A remark on finite element schemes for nearly incompressible elasticity, Computers & Mathematics with Applications 74 (9) (2017) 2047–2055.

[23] T. Hughes, Equivalence of finite elements for nearly-incompressible elasticity, Journal of Applied Mechanics 44 (1977) 181–183.

[24] I. Babuška, M. Suri, Locking effects in the finite element approximation of elasticity problems, Numerische Mathematik 62 (1) (1992) 439 – 463.

[25] I. Babuška, M. Suri, On locking and robustness in the finite element method, SIAM Journal on Numerical Analysis 29 (5) (1992) 1261–1293.

[26] M. Suri, Analytic and computational assessment of locking in the hp finite element method, Computer Methods in Applied Mechanics and Engineering 133 (1996) 347–371.

[27] P. E. Barbone, N. Nazari, I. Harari, Stabilized finite elements for time-harmonic waves in incompressible and nearly incompressible elastic solids, International Journal for Numerical Methods in Engineering 120 (8) (2019) 1027–1046.

[28] M. Chiumenti, Q. Valverde, C. A. de Saracibar, M. Cervera, A stabilized formulation for incompressible elasticity using linear displacement and pressure interpolations, Computer Methods in Applied Mechanics and Engineering 191 (46) (2002) 5253 – 5264.

[29] B. P. Lamichhane, A mixed finite element method for nearly incompressible elasticity and Stokes equations using primal and dual meshes with quadrilateral and hexahedral grids, Journal of Computational and Applied Mathematics 260 (2014) 356 – 363.

[30] F. Auricchio, L. B. da Veiga, C. Lovadina, A. Reali, An analysis of some mixed-enhanced finite element for plane linear elasticity, Computer Methods in Applied Mechanics and Engineering 194 (27) (2005) 2947 – 2968.

[31] G. Scovazzi, B. Carnes, X. Zeng, S. Rossi, A simple, stable, and accurate linear tetrahedral finite element for transient, nearly, and fully incompressible solid dynamics: a dynamic variational multiscale approach, International Journal for Numerical Methods in Engineering 106 (10) (2016) 799–839.

[32] C. Jiang, X. Han, G. Liu, Z.-Q. Zhang, G. Yang, G.-J. Gao, Smoothed finite element methods (S-FEMs) with polynomial pressure projection (P3) for incompressible solids, Engineering Analysis with Boundary Elements 84 (2017) 253–269.

[33] C. M. Goh, P. M. F. Nielsen, M. P. Nash, A stabilised mixed meshfree method for incompressible media: Application to linear elasticity and Stokes flow, Computer Methods in Applied Mechanics and Engineering 329 (2018) 575–598.

[34] A. Bermúdez, R. Durán, M. A. Muschietti, R. Rodríguez, J. Solomin, Finite element vibration analysis of fluid-solid systems without spurious modes, SIAM Journal on Numerical Analysis 32 (4) (1995) 1280–1295.

[35] A. Bermúdez, R. Durán, R. Rodríguez, Finite element solution of incompressible fluid-structure vibration problems, International Journal for Numerical Methods in Engineering 40 (1997) 1435–1448.

[36] S. Aimmanee, R. Batra, Analytical solution for vibration of an incompressible isotropic linear elastic rectangular plate, and frequencies missed in previous solutions, Journal of Sound and Vibration 302 (3) (2007) 613–620.

[37] R. Codina, Ö. Türk, Modal analysis of elastic vibrations of incompressible materials based on a variational multiscale finite element method, in: F. J. Vermolen, C. Vuik (Eds.), Numerical Mathematics and Advanced Applications ENUMATH 2019, Springer International Publishing, Cham, 2021, pp. 1021–1029.

[38] Ö. Türk, D. Boffi, R. Codina, A stabilized finite element method for the two-field and three-field Stokes eigenvalue problems, Computer Methods in Applied Mechanics and Engineering 310 (2016) 886 – 905.

[39] R. Codina, S. Badia, J. Baiges, J. Principe, *Variational Multiscale Methods in Computational Fluid Dynamics*, in Encyclopedia of Computational Mechanics (eds E. Stein, R. Borst and T. J. R. Hughes), John Wiley & Sons Ltd., 2017, pp. 1–28.

[40] R. Codina, Analysis of a stabilized finite element approximation of the Oseen equations using orthogonal subscales, Applied Numerical Mathematics 58 (3) (2008) 264–283.

[41] X.-B. Gao, G. H. Golub, L.-Z. Liao, Continuous methods for symmetric generalized eigenvalue problems, Linear Algebra and its Applications 428 (2) (2008) 676 – 696.

[42] I. Castañar, J. Baiges, R. Codina, A stabilized mixed finite element approximation for incompressible finite strain solid dynamics using a total Lagrangian formulation, Computer Methods in Applied Mechanics and Engineering 368 (2020) 113164.